Mechanical properties of polyisoprene-based elastomer composites

Journal:	*Macromolecules*
Manuscript ID	ma-2023-010849.R1
Manuscript Type:	Article
Date Submitted by the Author:	11-Sep-2023

Complete List of Authors:	Dhara, Deboleena; Columbia University, Chemical engineering Rahman, Md Anisur; Oak Ridge National Laboratory, Chemical Science Division Ruzicka, Eric; University of South Carolina, Chemistry Karekar, Akshay; Martin-Luther-Universität Halle-Wittenberg, Institut für Physik - NMR Vlassopoulos, Dimitris; Institute of Electronic Structure and Laser, IESL, Materials Science & Techn. Saalwächter, Kay; Martin-Luther-Universitat Halle-Wittenberg, Institut f. Physik Benicewicz, Brian; University of South Carolina, Chemistry and Biochemistry Kumar, Sanat; Columbia University, Department of Chemical Engineering

Mechanical properties of polyisoprene-based elastomer composites

Deboleena Dhara,[†] MD Anisur Rahman,[‡,§] Eric Ruzicka,[‡] Akshay Karekar,[#] Dimitris Vlassopoulos,[||,@] Kay Saalwa̲chter,[#] Brian Benicewicz,[‡] Sanat K Kumar[†,]*

[†]Department of Chemical Engineering, Columbia University, New York, New York, 10027, USA
[§]Chemical Science Division, Oakridge National Laboratory, Oakridge, Tennessee, 37830, USA
[‡]Department of Chemistry and Biochemistry, University of South Carolina, Columbia, South Carolina, 29208, USA
[#]Institut füur Physik, Martin-Luther-Universita̲t Halle-Wittenberg, 06099 Halle (Saale), Germany
[||]FORTH, Institute for Electronic Structure and Laser, Heraklion 70013, Greece
[@] University of Crete, Department of Materials Science & Technology, Heraklion 70013, Greece

Abstract

We have explored the origins of mechanical reinforcement in elastomers filled with polymer grafted nanoparticles (NPs). The brush chains are constructed from the same monomers as the polymer melt although they have different microstructures (i.e., different amounts of trans and cis isomers). The NPs display a variety of morphologies depending on variations in the graft density of the polymers, with these morphologies hardly changing when the matrix (and the grafts) are crosslinked using dicumyl peroxide (DCP). NMR measurements show that the crosslink densities depend only on the DCP content and are independent of NP morphologies. We find that the elastic moduli of these materials are strongly dependent on the NP morphology but that the maximum reinforcement occurs when the NPs percolate, but in a manner where the cores are exposed enough to have strong enthalpic interactions – these interactions could either be due to direct core-core van der Waals attractions or due to bridging interactions driven by polymers adsorbed on adjacent NPs. The nonlinear mechanical response of these materials are less sensitive to changes in NP morphology and loading. These results emphasize the important role of the exposed NP surface in determining the moduli of crosslinked elastomers. This last aspect is apparently less relevant for the corresponding uncrosslinked melts filled with NPs.

For Table of Contents Use Only

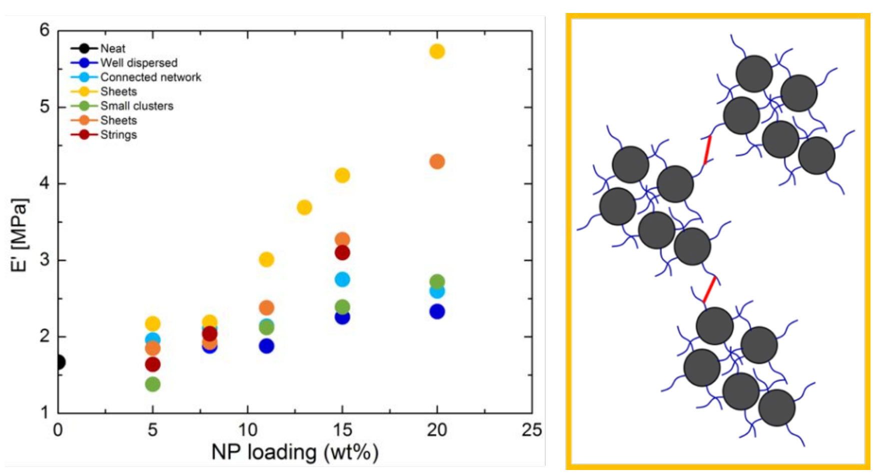

1. Introduction

Crosslinked elastomers are generally reinforced with nanofiller to achieve the mechanical properties necessary for applications, especially in the tire industry. Thus, the introduction of silica nanoparticles into crosslinked rubbers can improve rolling resistance, directly affecting fuel economy and impacts on the environment.[1, 2] The role of the NPs is to reinforce the polymer matrix and improve fracture and abrasion properties. The origins of the reinforcement mechanism by the addition of NPs has been an ongoing discussion for decades - several mechanisms related to *filler networking* have been proposed to understand it.[3-6]

Filler networking can be established by at least two different mechanisms: (i) direct *filler-filler association* caused due to direct short-range van der Waals forces; (ii) chain-mediated *filler-polymer association* arising from chain bridging, adsorption and confinement.[7-9] In scenario (i) reinforcement relies on direct filler-filler interactions, where filler agglomeration/network formation are responsible for high levels of reinforcement and transmission of stress across a sample occurs through a rigid filler network.[10-12] In support of scenario (ii) Zhu et.al. found that long matrix chains are uniformly adsorbed on the NPs; when a chain is simultaneously adsorbed on to two NPs, i.e., when chain bridging occurs, this then is the first step to NP percolation as proposed theoretically.[13] The presence of these adsorbed chains made the sample more resistant to stress-induced destruction of filler networking.[14] Trapped entanglements as a result of strong filler-polymer interactions result in substantial reinforcement and release of these entanglements lead to loss in dynamic moduli.[15] In highly filled elastomer composites it has been shown that "glassy" (immobilized) rubber bridges become part of the filler network and the dynamics of the yield and rebirth of the bridges account for the observed dissipative properties.[16-22] However, distinguishing and quantifying the relative contributions of the various (physical) mechanisms that can explain the mechanical reinforcement in filled elastomers is an experimental and theoretical challenge.[13]

The linear and nonlinear mechanical properties as functions of frequency and temperature and the relative contribution of various reinforcement mechanisms are dictated by the microscopic structure of the NP-based network.[23-26] Hence, it is important to have the ability to determine and control NP dispersion state *a priori* to potentially derive the critical insights into reinforcement mechanisms. Various strategies have been developed to incorporate silica fillers into an elastomer matrix, e.g., melt mixing, using coupling agents, coating agents and functionalized polymer chains.[27-31] Berriott et.al. prepared crosslinked elastomer composites by dispersing fumed silica suspensions in monomer/crosslinker mixtures and simultaneously carrying out polymerization and crosslinking reactions.[32] Such *in situ* approaches are strongly limited by the reaction kinetics of chains bonded to the NP surfaces, making it difficult to control NP dispersion.[33] Pregrafting polymers onto the NPs can help to control dispersion by tuning the graft density, and matrix and graft chain length.[33, 34] Much of the prior work with grafted NPs have been performed on composites in the melt state.[35-39] On comparing the reinforcement in uncrosslinked composites across different morphologies, Moll *et al.* , Akcora *et al.* and Dhara *et al.* noticed a (nonmonotonic) dependence of mechanical reinforcement with changing NP morphologies.[40-42] At the same NP loading, percolating NP sheets displayed solid-like mechanical behavior at lower particle loadings than ones with uniform NP dispersion. To our knowledge, the only example of crosslinked elastomers using grafted NPs was reported by Abbas et al.[43] although there are many worked with bare NPs, e.g., ref 44. Abbas et al compared the solid state mechanical properties of polychloroprene composites across two graft densities and observed that composites with low graft density and molecular weights showed higher mechanical reinforcement. The molecular (morphological) drivers of this result are not established.

In our previous work, we studied the long-time shear mechanical response of melt-state composites with three different NP morphologies (well dispersed, connected network, sheets) formed by mixing polyisoprene homopolymers with polyisoprene grafted silica particles. Our results showed that maximum mechanical reinforcement occurs for the sample with intermediate grafting density NPs which formed a connected network, where NP percolation mediated by the graft chains allows for stress propagation across the system.[41] In this work, we expand on this study and investigate an array of morphologies from well dispersed to different degrees of aggregation, but this time in the crosslinked state. It is important here to note that our earlier melt state mechanical measurements were conducted in a shear mode, while the current solid-state experiments use tensile deformation. These different protocols, which might cause some small variations to the results, need to be remembered when we draw mechanistic conclusions from our studies. To gain deeper insights into the reinforcement mechanism of crosslinked elastomer nanocomposites, we ask the following questions: (1) How do NP morphologies change on crosslinking? (2) Which morphology yields the highest reinforcement in the linear and nonlinear regimes? Is it directly correlated to the degree of aggregation? (3) Does the reinforcement mechanism change with NP morphologies?

A combination of complementary experimental techniques, i.e., small angle X ray scattering (SAXS), dynamic mechanical analysis (DMA), tensile stress-strain measurements and nuclear magnetic resonance (NMR), allows for a detailed characterization of the structure and properties of these composites. The macroscale mechanical properties were compared with the molecular-scale information obtained by NMR and SAXS. We find that the differences in NP structural organization have a large impact on the modulus enhancement in the linear response regime. The morphology with the maximum shear reinforcement in the melt state does not show the same enhanced properties in the crosslinked state under tension – instead, the percolated morphology where NP cores are in contact yields the maximum tensile modulus. By delineating the interplay of filler-filler and filler-polymer interactions, we attempt to understand the source of reinforcement for the different morphologies across the melt and crosslinked states, with the caveat that these are under different deformation protocols.

2. Materials and Methods

2.1 Materials

Spherical nanoparticles (MEK-ST) of diameter 14 $\pm$ 4nm were provided by Nissan Chemical Company. Polyisoprene (75% 1,4 cis) with a molecular weight of 35kDa obtained from Sigma Aldrich was used as the matrix. Note that the graft PI chains had 75% 1.4 sequences, and 20% 1,2 content. In contrast the free PI chains, from Sigma, had 24.8% 1,4 and 75.2% 1,2 isomers. This difference in chain microstructure between the graft chains and matrix polymer, however, does not substantially affect the morphologies that result relative to situations where the matrix and graft have identical structures.[33] Dicumyl peroxide (99% purity), used as the crosslinking agent, was also obtained from Sigma Aldrich.

2.2 Sample preparation

The grafted NPs were synthesized using the RAFT protocol.[45] (This grafting-to protocol is discussed in our earlier publications.[33, 41]) Free matrix chains were dissolved in THF at 5wt% and vortexed for 2 hours at room temperature.

The grafted NPs were added to the polymer solution at 5, 8, 11, 15, 20 wt% of the nanoparticle core to the total mass of polymer plus NP, respectively. Dicumyl peroxide solution is added at 10wt% of the total polymer (graft +free) mass. The resulting mixture was vortexed vigorously and probe sonicated before allowing the THF to evaporate under vacuum for 3 days, again at room temperature. The samples were then melt pressed at 160^{o}C for 20min to obtain vulcanized rubber sheets of desired thicknesses and shapes.

2.3 Sample characterization

2.3.1 Small Angle X Ray Scattering

Small angle X ray scattering was performed at room temperature under vacuum on a SAXSLAB Ganesha instrument at the Columbia Soft Matter Laboratory with a Cu Kα source (λ = 1.54 Å), a Pilatus 300K detector, and a variable sample to detector distance that covers a q range of 0.004 – 1.2 Å^{-1}. 2D scattering patterns were integrated using the SAXSLAB's saxsgui software to obtain obtain one dimensional scattering curves of the intensity of the scattered radiation (background-subtracted) I as a function of q.

2.3.2 Transmission Electron Microscopy

Samples were cut from an un-crosslinked melt using cryo-ultramicrotomy (Leica EM FCS) at -90^{0}C with cut speeds varying between 2 and 10mm/s to obtain sections of thickness ~100nm. The sections were then collected on a Formvar-coated copper grid and stored in liquid nitrogen. They were then imaged on an FEI Talos 120^{0}C TEM at 120 kV, equipped with a Gatan OneView camera.

2.3.3 Dynamic Mechanical Analysis

Dynamic mechanical analysis was performed on DMA 800 (TA Instruments) in tension mode to obtain the Young's modulus, toughness (the area under the stress-strain curve), tensile strength at break and failure strain. Temperature sweeps were run from -80^{o}C to 60^{o}C at a heating rate of 3^{o}C/min under nitrogen flow. A preload force of 0.05N was applied and tests were done at 0.03% strain and 1Hz frequency. The preload force induced a prestretch that was necessary to reduce the transmitted force in the vertical plane and avoid sample being ripped off from the two ends (grips). The 0.03% strain was chosen after performing strain sweeps to ensure that the tests were performed in the linear regime. The measured stress was the engineering tensile stress.

2.3.4 Stress-Strain Analysis

Tensile tests were carried out using Chatillon CS2 universal testing machine, equipped with a 500N load cell. The crosshead speed was 10mm/min. Samples were molded into standard dogbone shapes of 0.4mm thickness and 42mm length (dimensions were chosen based on the ASTM D412 standards). Only the rectangular neck region (~ 18 mm) was exposed between the grips. A minimum of 3 measurements were recorded, and the average values were reported. The tests where the samples failed prematurely at the grips have not been included in the averages.

2.3.5 NMR

Static low field time-domain double-quantum (DQ) ^{1}H NMR experiments were performed on a Bruker minispec mq20 spectrometer, which has a resonance frequency of 19.95 MHz corresponding to a magnetic field strength of about 0.47 T. The spectrometer probe has a 90° pulse length of 2.7 μs. Molded discs of 2 mm thickness and 8 mm diameter were stacked to a height of 4 mm in an NMR glass tube and maintained at 80 °C by a BVT 3000 temperature controller.

3. Results

It is appropriate first of all to compare DCP-vulcanized rubbers relative to sulfur crosslinked materials. The DCP crosslinked materials are "cleaner", as one can go without all the messy additives, resulting in samples suitable for scattering experiments. But the actual rubber matrix is by tendency more **in**homogeneous. Sulfur vulcanization results in topologically more homogeneous, defect-poorer systems, see ref 46. Earlier more indirect work claimed the contrary, but Saalwächter and co-workers disproved this (based on the strain-induced crystallization behavior).[47] Hence we pick DCP crosslinked materials as a route to obtaining samples more homogeneous and amenable to the experiments performed here.

First, we gradually change the DCP loading in the neat polymer, and study how it affects mechanical properties. This in turn helps us determine the optimal DCP loading. We then turn to understanding NP morphologies in the melt state and how they evolve on crosslinking with this optimal DCP crosslinker loading. The tensile mechanical properties of the composites in the linear and nonlinear regime help us determine which morphology gives us the highest reinforcement.

After studying the macroscale mechanical properties, we used DQ NMR spectroscopy to assess the crosslink density in the polymer phase and better understand the reinforcement mechanism.

Table 1: Polyisoprene Grafting Parameters. X is the overcrowding parameter and S* is the polymer surface coverage of the NPs

Sample	Graft M_w (kDa)	Grafting density (σ) (ch/nm^2)	P/N $\equiv$ $1/\alpha$	X	Morphology	S^*	Color Code
A	38	0.25	0.9	1.01	Well dispersed	1.00	Dark blue
B	20	0.15	1.8	0.82	Connected network	1.00	Light blue
C	68	0.06	0.51	0.31	Strings	1.00	Red
D	32	0.035	1.1	0.23	Sheets	0.95	Yellow
E	42	0.015	0.83	0.11	Sheets	0.8	Orange
F	156	0.007	0.22	0.05	Small clusters	0.69	Green

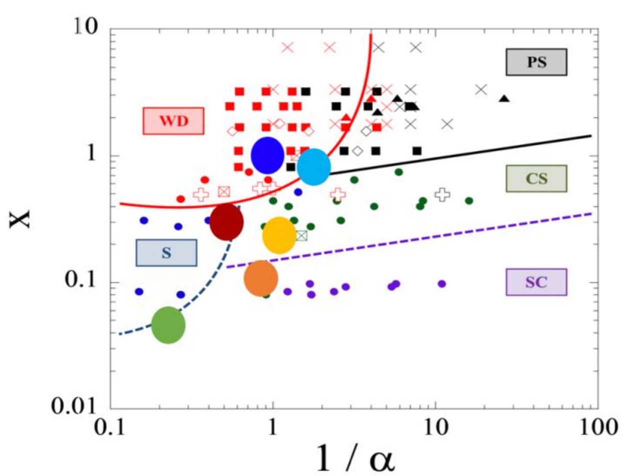

Figure 1: Morphology plot showing the dispersion of homopolymer-grafted NPs in a homopolymer matrix, compiled by Kumar et al. from experimental data in literature (WD: well dispersed, PS: phase separated, S: strings, CS: connected sheets, SC: small clusters).[48] The y and x axis represent spherical brush overcrowding parameter (X) and melt to brush chain length ratio ($1/\alpha$). On the same plot, we overlay the primary systems studied in this work.

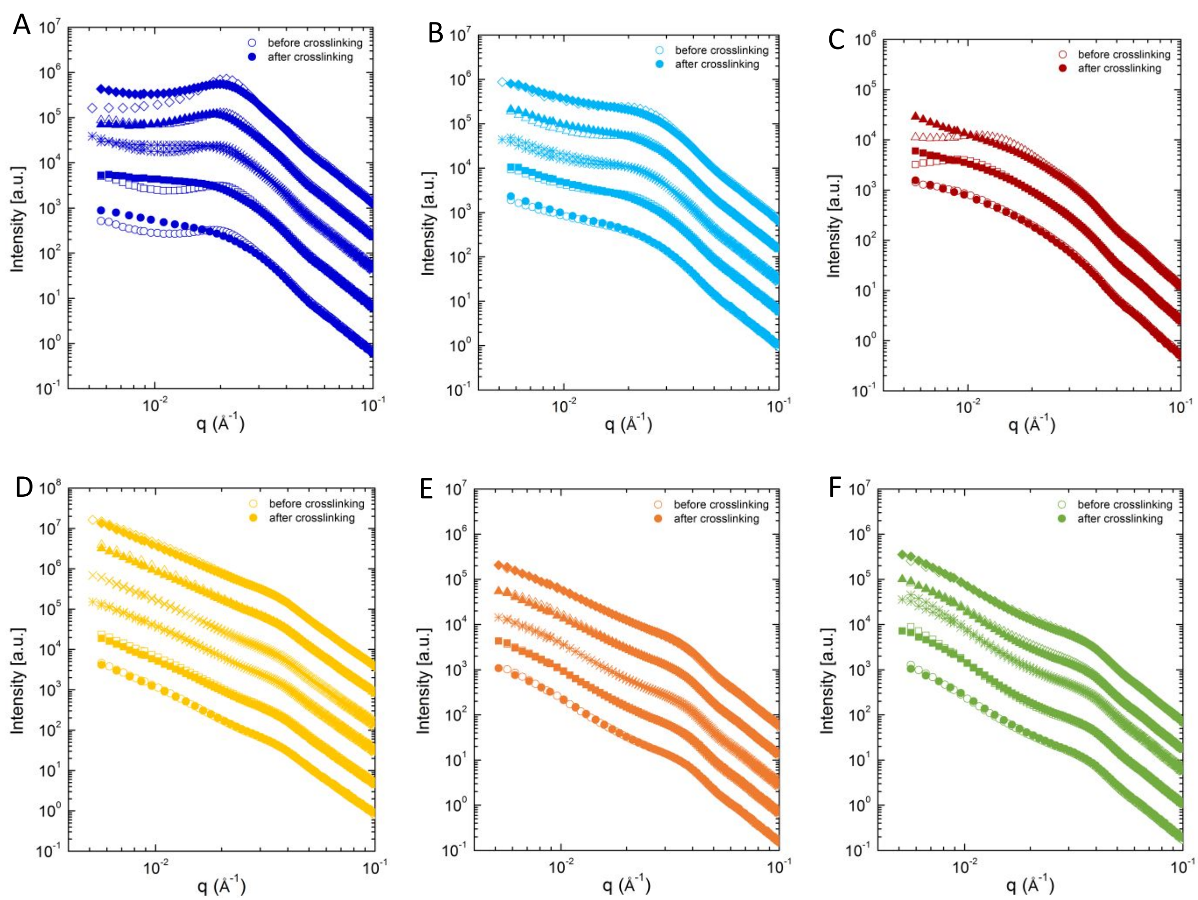

Figure 2: SAXS curves before (open symbols) and after (filled symbols) crosslinking for the different morphologies at different NP loadings (circle: 5wt%, square: 8wt%, star: 11wt%, cross: 13wt%, triangle: 15wt%, diamond: 20wt%). The different colored plots correspond to the different samples shown in figure 1.

3.1 Morphology studies

The morphology plot in Figure 1 is a common reference point to determine *a priori* the NP dispersion state when polymer-grafted NPs are mixed with a polymer matrix of essentially the same chemistry.[48, 49] The data in this Figure is a compilation from a variety of polymeric systems but is largely dominated by the (athermal system of) PS-g-silica in a PS matrix, with a NP loading of 5 wt%. We have done some work on enunciating the role of NP loading on the morphology of the materials, but mainly through their consequences on mechanical response. For example, roughly 15 years ago[40] we had considered the rheological properties of the nanocomposites as a function of NP loading. We considered two states of dispersion – i.e., well-dispersed and percolating NP sheets at 5 wt% of the NPs – and then varied NP loading. Indeed, while the sheet structure is already percolated at 5 wt% NP, the well-dispersed state also becomes percolating at 15 wt% NP loading. Thus, dispersion states change with loading, but characterizing this is difficult since electron microscopy no longer can be used at high loading. Also, the SAXS patterns become less able to distinguish between these states at higher NP loadings.

The overcrowding parameter (X) is the ratio of the actual number of grafted chains on a NP to the number of chains that occupy the same volume as the grafted NPs in an unperturbed melt.[50] Note that this refers to the property of a single NP – as we have discussed above the role of NP loading is not fully enunciated and hence we do not have a parameter that accounts unambiguously for this variable. We have previously shown that this morphology plot is also relevant to polyisoprene based systems in the melt state, where graft and matrix have the same monomer building blocks but do not have the same microstructure.[33, 41] We extend this previous study to a broader range of samples and study the role of crosslinking.

The polymer-grafted NPs display different morphologies depending on the graft density and ratio of graft to matrix chain length, as shown in Table 1. These melt NP structures, determined by TEM and SAXS, closely match expectations from what is known about this class of grafted NPs in corresponding melts. Scattering data are shown in Figure 2 for the different morphologies at various NP loadings before and after crosslinking. For the highest graft density tested ($X \approx 1$), sample A shows well dispersed structures across different NP loadings, as evident from the TEM and SAXS curves and as expected. Here the core-core attractions are screened by the dense brush.

The interparticle spacing gets altered on crosslinking and the peak becomes more smeared, but the well dispersed morphology is apparently maintained. As we lower the graft density, the X value decreases, softening the brush-brush repulsion and allowing different morphologies to form (strings/percolated network/sheets).[34] Sample B forms a percolated NP network (low q scaling exponent ≈ 1.5), that remains essentially unchanged on crosslinking. At the intermediate graft density, the particles self-assemble to form strings (sample C) at low $1/\alpha$ and connected sheets (sample D,E) at high $1/\alpha$.[37] Sample C, at the boundary of sheets and strings is prone to aggregation at high loadings after crosslinking. Samples D and E, which have progressively lower X values, show highly aggregated sheet-like structures with a sharp scattering upturn at low q with a $I \sim q^{-2}$ dependence. This power law is consistent with the sheet-like structure forming. The TEM image for sample D corresponds well with the SAXS pattern and suggests that the NPs are in intimate contact in a cluster [see supplementary information]. While both D and E show the same low q scaling, the degree of aggregation is slightly different due to the different graft parameters. Sample F lies well within the small cluster phase. Here the graft density is so low that core-core attractions dominate the self-assembly behavior and the NPs form small clusters. The latter three samples display no changes in structure on crosslinking. Overall, except at the highest X, where the interparticle spacing between NPs gets affected by crosslinking, an effect more prominent at high particle loadings, the morphologies are independent of the process of crosslinking for all other X.

To further quantify these ideas, we estimate the polymer surface coverage (S^*), which represents the fraction of the silica surface that is covered by the graft polymer. This area is excluded to the exposed cores of adjacent NPs due to the grafted layer. This equation for S^* was introduced by Asai et al.[51, 52] As explained in these papers, this expression was derived by analogy to random sequential adsorption. So, schematically, this involves thinking of the process of creating a grafted NP by adsorbing one chain at a time on to the NP surface. Each canopy chain then covers some part of the surface. The calculation of S^* will give us a qualitative estimate of the strength of the core-core attractions:

$$S^* = 1 - \exp\left(-f\frac{R/r}{2(1+R/r)}\right)$$

where, f is the number of grafts and $r = 7nm$ is the NP radius. Using $R \approx 0.87 R_g f^{-1/5}$ and $R_g \approx 0.9(N/6)^{1/2}$, where N is the ratio of molecular weight of graft to Kuhn monomer, we calculate S* for the different morphologies having $\sigma \sim 0.007 - 0.25\ \text{chains/nm}^2$ (Table 1).[49] The limits $S^* = 0$ and $S^* = 1$ correspond to ungrafted and densely grafted silica, respectively. The regime $0 < S^* < 1$ corresponds to sparsely grafted NPs. At the high X limit (samples A, B and C), we observe $S^* = 1$, indicating that the surface is completely covered by the dense brush – in these cases the decreasing X only reduces the brush overcrowding and hence the brush-brush repulsion. The attractive particle core-core interactions are thus completely screened. As we lower the X values, we observe that S^* decreases progressively. In these last three cases (samples D, E and F) the attractive inter NP core van der Waals attractions become progressively more pronounced.

3.2 Mechanical properties

The mechanical properties as derived from small amplitude oscillatory shear and creep measurements of polymer grafted NPs in a polymer melt display maximum reinforcement when

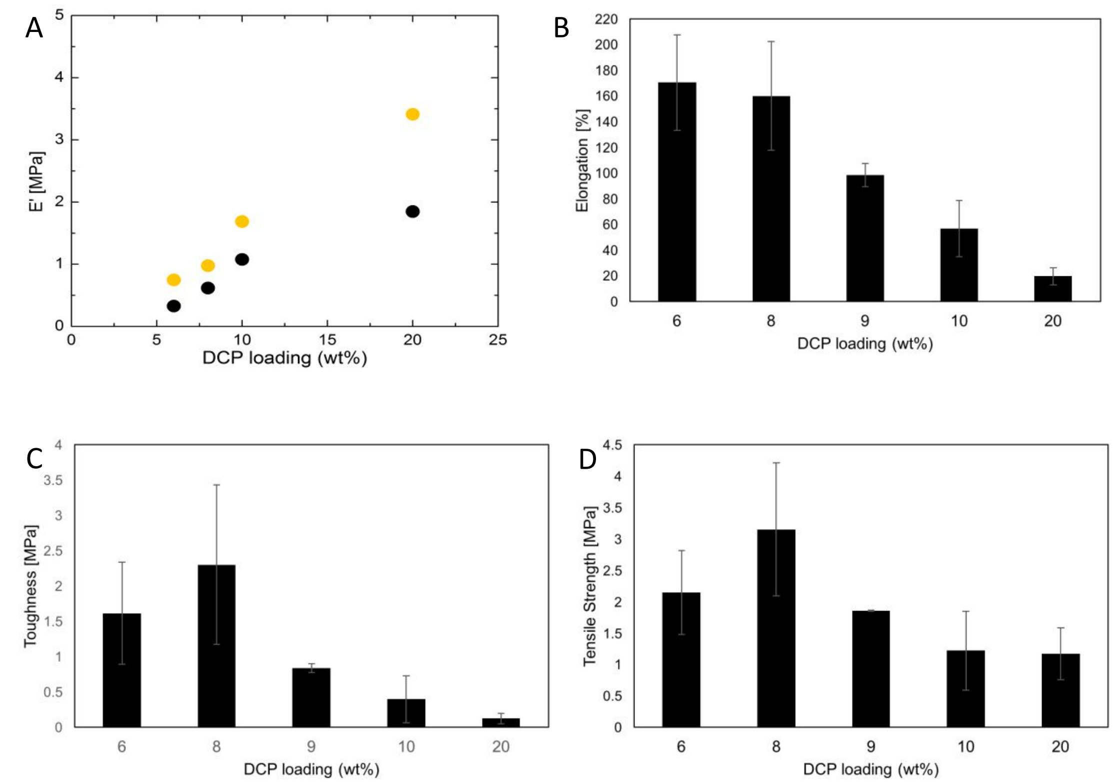

Figure 3: (A) Storage modulus of neat and sample S with 5wt% NP loading containing 6wt%, 8wt%, 10wt% and 20wt% DCP. (B,C,D) Elongation at break, toughness and tensile strength of neat PI at different levels of DCP loading, respectively.

the NPs form a percolated network.[42] Zaid *et al*. showed that for crosslinked polymer nanocomposites systems high grafted molecular weights and low graft densities enhanced the tensile properties more than low grafted molecular weights and high graft densities.[43] We go beyond the Zaid *et al*. results and show that mechanical reinforcement under tensile deformation is most influenced by two factors: (i) whether the NP structure is percolated or not and (ii) that for percolated structure, the ones with most attractive interactions show increased reinforcement. This reinforcement shows a non-monotonic dependence on graft density, σ, with a maximum occurring at an intermediate $\sigma \approx 0.035$ chains/nm^2, i.e., where $X \approx$ 0.6-0.8 - here the NPs form percolated structures but van der Waals attractions between the cores also play a significant role.

Temperature sweeps in the linear regime help us delineate the high temperature/low frequency hysteresis that contributes to rolling resistance and low temperature/high frequency hysteresis that determines the wet grip of tires. We gradually increase the concentration of DCP and find that the reinforcement, as characterized by the Young modulus, increases systematically for both the neat polymer and sample S containing 5% NP, Figure 3A. To thus determine the optimal DCP content to operate at, we consider the tensile mechanical properties of the neat polymer with different concentrations of DCP in the nonlinear regime. The stress-strain curve of rubber materials is usually linear over a fairly large range of strain.[53, 54] The elongation at break, toughness and tensile strength are derived from the true stress vs strain graph [Figures 3 B,C,D].[55] While the neat polymer shows an increase in modulus and decrease in elongation at break with increases in DCP loadings, we observe that tensile strength and toughness have a non-monotonic dependence. Samples with 8% DCP loadings show the highest values in tensile strength and toughness. Though samples with 20% DCP showed significantly higher linear reinforcement, they have very poor nonlinear properties- namely elongation to break and hence toughness. Hence, as a compromise,s we kept the DCP loading constant at 10wt% for the subsequent tests with the composites.

While all the composites (with very different NP dispersion states) behaved similarly in the glassy regime, a result that has been observed previously by Maillard *et al*., we observed significant differences in modulus enhancement for the different morphologies in the rubbery regime, an effect more prominent at higher loadings [Figure 4].[56] For simplicity, we compare the data at 30^{o}C in the rubber plateau region [Figure 4C]. At lower NP loadings (< 10%), the reinforcement is essentially independent of morphology; the modulus, however, is similar to that of the neat crosslinked polymer. As the filler fraction increases beyond 10wt%, however, we observe significant differences in mechanical reinforcement among the different morphologies.[57] In the limits of high or low graft density (samples A,B,F), we observe minimal reinforcement, even at the highest NP loading. These samples show behavior similar to that predicted by the Guth-Gold model.[58] Interestingly, in the intermediate graft density region, we see significant reinforcement.

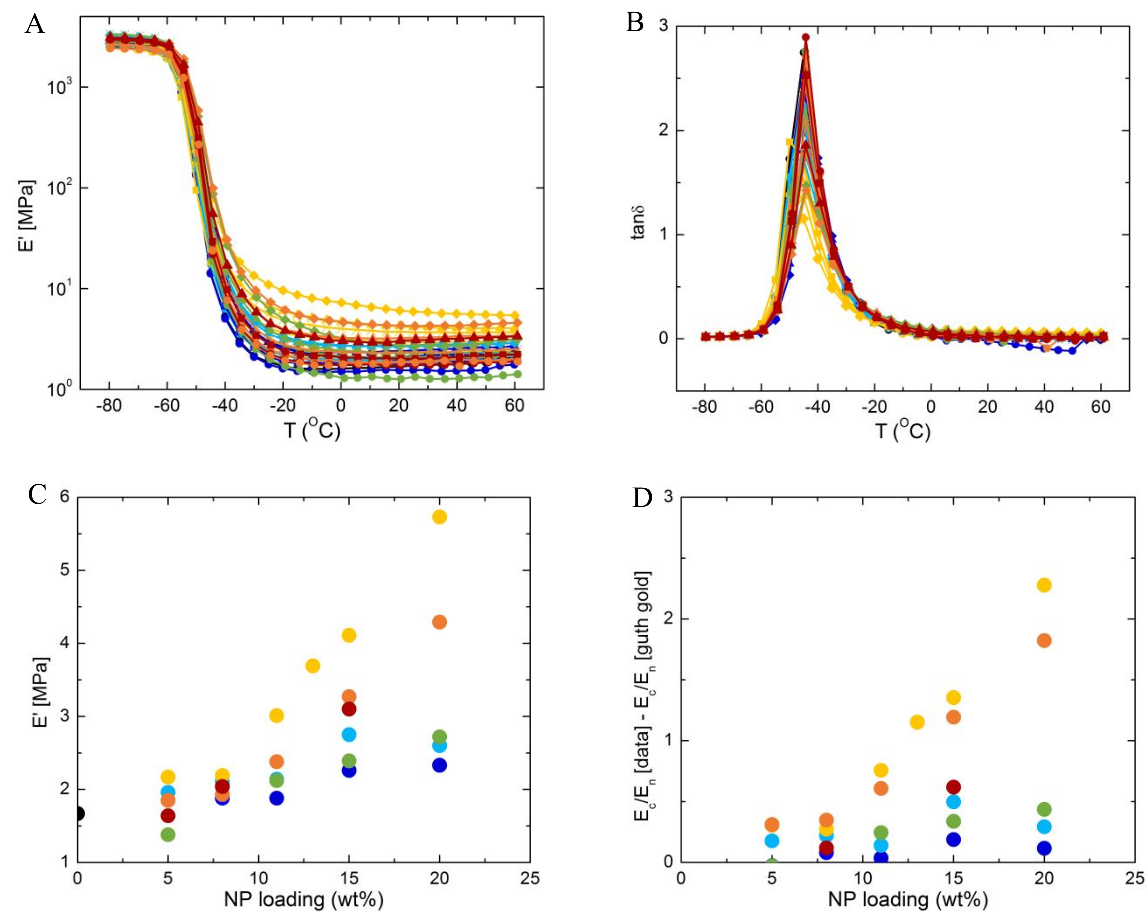

Figure 4. (A) Storage modulus and (B) tan δ of neat polymer and filled composites with different NP loadings (circle: 5wt%, square: 8wt%, star: 11wt%, cross: 13wt%, triangle: 15wt%, diamond: 20wt%). (C) Storage modulus of the composites at 30C. (D) Modulus enhancement (E_c/E_n) of the filled composites after subtracting the prediction from Guth-Gold. The plots are color coded to represent the different samples, as shown in figure 1.

The highest enhancement is shown by sample D, followed by E. Interestingly, the Young's modulus of sample D decreases with temperature at 20wt% loading (Figure 4A); all other samples show moduli increases with increasing temperature in the regime above the glass transition temperature of the PI. The samples that show modulus increases with temperature are dominated by the entropic elasticity of crosslinked networks.[4] On the other hand, a decreasing modulus with increasing temperature implies that an enthalpic effect plays the more important role. Saalwächter et.al. attributed this decrease in modulus to the softening of immobilized polymer bridges with locally increased T_g.[19, 59] In the same vein, it is also possible that the enthalpic interactions could also result from the van der Waals attractions which manifest when bare NP cores contact each other. Which of these two effects dominate is unclear to us, but it is apparent that enthalpic effects are key to the mechanical response of the samples that demonstrate the largest reinforcement.

We explore these ideas further here. The filler contribution depends strongly on the NP structure and is dictated by the interaction between the particle cores as well as the brush repulsions.[60] The reinforcement shown by the composites is a combination of different effects:[5] (i) the contribution of the crosslinked network (crosslink density in the polymer phase), (ii) the effect of adding fillers as predicted by the Guth-Gold model, (iii) filler-filler interactions (dictated by morphology), (iv) filler-polymer interactions (dictated by the brush). The increase in modulus due to point (ii) for particle reinforced elastomers is:

$$\frac{E_c}{E_n} = 1 + 2.5\varphi + 5\varphi^2 \qquad (1)$$

where E_c and E_n are the tensile moduli of the filled and unfilled composites, respectively.[58, 61] Three comments are particularly germane here: (1) The fitting model is based on independent particles, not clusters. (2) Imperfections (heterogeneity, dangling ends) certainly play a role here but these effects are ignored. (3) In Baeza et al. (dfferent system but interconnected NPs) we used the Doolittle equation to descript the large increase of modulus with loading.[62] To understand the role of morphology, we normalize the composite's modulus by that of the neat polymer and subtract the Guth-Gold contribution, Figure 4D. Any remaining reinforcement must be associated with filler-filler and filler-polymer interactions. Only samples D and E show modulus enhancements. This enhanced reinforcement can be attributed to the formation of sheet like NP structures. Note that these are precisely the two samples that show a decreasing modulus with increasing temperature, implying that the enhanced reinforcement in these cases is always enthalpic in origin. The reinforcement peaks in this X region and decreases as we move away from this belt ($X \sim 0.1\ to\ 0.25$). The percolation threshold of D and E is similar (~8wt%), much lower than the other composites lying outside this belt. The load carrying capacity of the filler networks peaks for D, an effect more prominent at higher loadings again suggesting that enthalpic inter NP interactions (either though adsorbed glassy chains or due to core-core van der Waals interactions) dominate the elastic mechanical response of these networks. This result is the most significant new finding of the current work.

It is apparent that toughness, tensile strength and elongation at break remain effectively constant across morphologies and NP loadings, as shown in Figure 5. These numbers, in each case, are larger than the corresponding crosslinked pure PI, implying that the NPs have a positive effect on nonlinear properties but that these increases are independent of the NP morphology and also loading. CN appears to have slightly higher toughness, tensile strength and elongation at 5wt% NP loading [Note: the error bars for CN at 5wt% loading are significantly larger than for the other samples.] This is in dramatic contrast to results in the linear regime, where NPs forming sheet like structures yield the optimal mechanical reinforcement. Apparently, what is important is that NPs

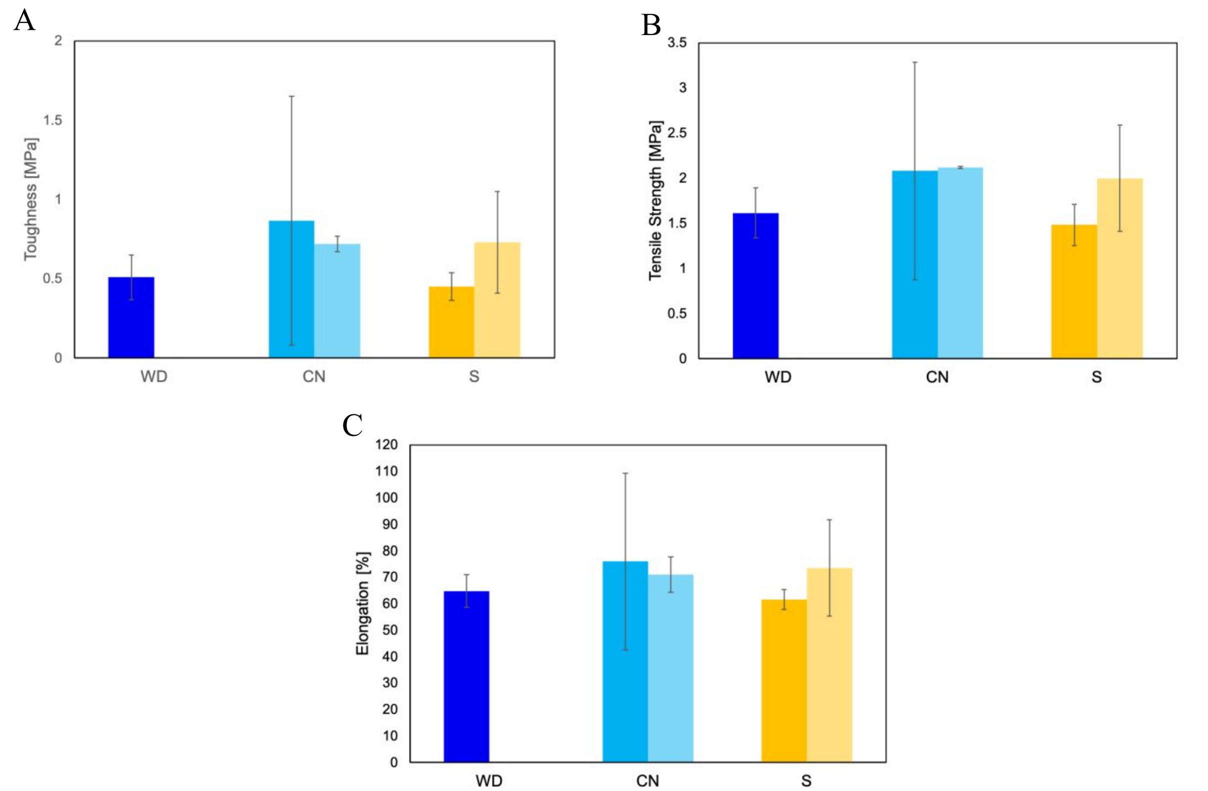

Figure 5: (A) Toughness, (B) Tensile strength and (C) Elongation at break for samples A, B, D at 5 wt% (dark color) and 11 wt% (lighter color) NP loading.

act as additional network junctions but that these effects are not dependent on the filler morphology. The enthalpic interactions driven by either NP-NP van der Waals interactions or glassy bridges are not the most dominant determinant of this nonlinear mechanical response.

3.3 Crosslink densities of the rubber matrix

In the previous sections, we saw that samples forming aggregated sheet like structures showed the highest reinforcement and appeared to be percolated at much lower NP loadings. Macroscopic mechanical properties themselves are not sufficient to understand the microscopic mechanism of rubber reinforcement. We use double quantum NMR spectroscopy to quantify the crosslink density of the rubber phase and the fraction of elastically inactive defects to enunciate this underpinning microscopic picture.[4]

In elastomers, topological constraints like entanglements and crosslinks lead to anisotropic chain segmental motions and, thus, their partial averaging. The magnitude of these constrained motions can be measured by the residual dipolar coupling constant (D_{res}). This is connected to the segmental dynamic order parameter and is a measure of the crosslink density.[63] A NMR experiment based on a multiple-quantum (MQ) pulse sequence gives a double-quantum (DQ) signal (I_{DQ}) that contains information related to constrained segments, and a reference signal (I_{ref}) that contains relaxation-induced details. In the long-time limit, these signals decay to zero (figure 6A).[64] By an adequate normalization of the DQ signal derived through a point-by-point division by the sum of the two signals, a normalized DQ build-up curve (I_{nDQ}) is obtained. This procedure also enables accounting for the presence of any defects (loops, dangling chains, and sol), usually by a single or a two-component exponential decay fit to the 'sum' signal. By using a suitable fitting function, the magnitude of D_{res} and its distribution throughout the volume of the sample can be obtained. Figure 6A gives an overlay of these three signals for sample A at 5 wt% NP loading. The fits are performed using a function that considers a log-normal distribution of couplings.[65] This yields a median value of D_{res} (D_{med}) and its corresponding distribution (σ_{ln}), the latter being a dimensionless quantity.

In the context of residual dipolar coupling, chain segments adsorbed on the filler surface are expected to demonstrate a much high static limit coupling D_{stat}, much higher than the D_{res} of the matrix. This contribution, in fact is better quantified by the more simple and quantitative free-induction decay (FID) analysis, and shows up as little initial step-up in the DQ signal. This

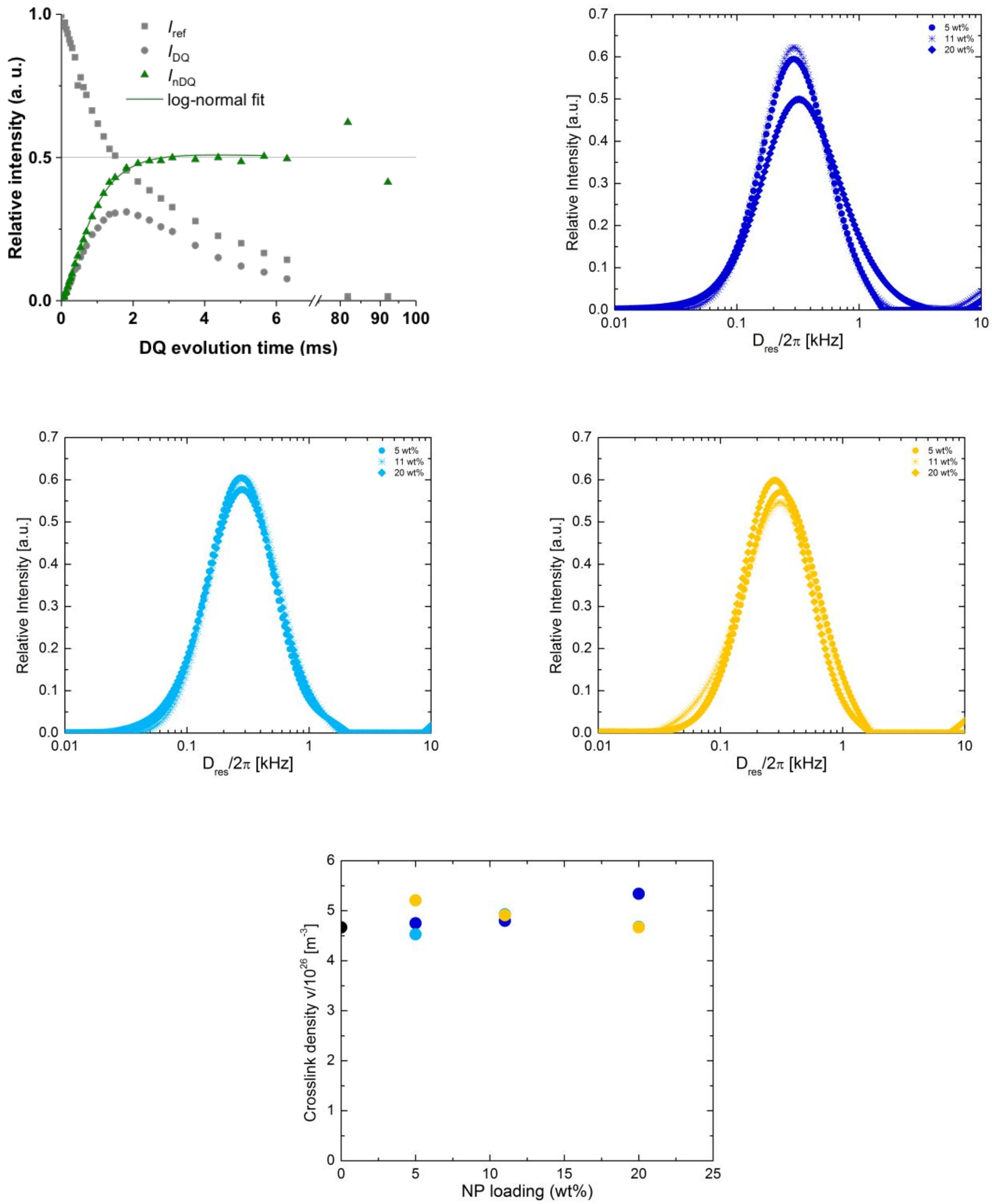

Figure 6: (A) fit to the normalized double-quantum (DQ) build-up signal (I_{nDQ}) for sample A with 5 wt% NP, obtained after processing the reference (I_{ref}) and DQ (I_{DQ}) signals. The slope of the I_{nDQ} signal is a measure of crosslink density encoding D_{res}. (B),(C),(D) The distributions of crosslink density (in "NMR units" of D_{res}), obtained by regularization of the corresponding I_{nDQ} signals, are represented for three different morphologies. (E) Crosslink density for the different morphologies. Note: the plots are color coded as follows: A-dark blue, B-light blue, D-yellow

component was found to be rather small in our samples. However, a small amount may play a significant role in reinforcement.[19] In the current set of samples, D_{res} reflects contributions from crosslinks and entanglements usually in an additive fashion:

$$D_{res} \propto \frac{1}{M_c} + \frac{1}{M_e} \quad (2)$$

where M_c, and $M_{e,}$ and M_{graft} are the crosslink, and entanglement molecular weights, respectively. In addition, in a region of order R_g of the grafted chains, D_{res} could be further increased due to the surface tethering and local stretching of the brush chains. This may thus lead to a high D_{res} tail of an inhomogenous D_{res} distribution. To accommodate for a small contribution from an immobilized surface layer, a bimodal fitting function is used, wherein the constrained fraction is force-fitted to a coupling value of 10 kHz and corresponding distribution width of 0.5.[66] These two values are adequately chosen based on the quality of the fit and account for a mobility gradient. Since this first component was very small and varied nonsystematically, we will not discuss it further. The second component of the fitting function encompasses the matrix-related effects, which will be discussed in detail here.

As an alternative to the fitting as described above, and to confirm the assumption of essentially unimodal D_{res} distributions (plus the minute immobilized layer contribution at ~10kHz, Figure 6 presents a visual representation of the residual dipolar coupling and its distribution obtained by Fast-Tikhonov regularization (*ftikreg*) of the I_{nDQ} signals for samples A, B, and D at 5, 11, and 20 wt% NP loading.[67] The measured distribution width for all the samples is about 0.600 on average. For homogeneous spin systems, such as homopolymers (polyisoprene in this case), a narrow distribution ($\sigma_{ln} \approx 0.1$) of crosslinks is usually expected, especially with sulfur as the crosslinking agent. However, it has been established that DCP tends to produce crosslinks with different chain lengths due to side reactions, thus leading to a broad distribution of crosslink densities.[68]

Samples with the well dispersed morphology (sample A) demonstrate an increase in D_{med} from about 0.280 kHz (at 5 wt% NP loading) to about 0.320 kHz (at 20 wt% NP loading). On the other hand, sample D shows an opposite trend from 0.305 kHz (at 5 wt% NP loading) down to 0.270 kHz (at 20 wt% NP loading). This is probably indicative of the deactivation of DCP by adsorption on available filler surfaces, thus depriving the matrix of the crosslinker. Interestingly, sample B exhibits no specific trend in accordance with the filler loading, with an average coupling value of about 0.275 kHz. At the higher filler loadings, all morphology types indicate the presence of noted minor amounts (about 3 %) of the highly constrained components corresponding to 10 kHz due to polymer-filler interactions, as seen from the small upturns at the highest coupling limit. The non load - bearing defect fraction averaged to 14 % across all samples.

We further estimate the cross-link density of the composites by combining the measurements of NMR and mechanical properties.[4, 69] We take the rubbery plateau modulus from temperature dependent DMA data for the unfilled neat polymer with variable amounts of DCP. The modulus values for the neat samples are in line with the D_{res} values obtained independently from DQ NMR measurements [see supporting information]. This allows us to determine the proportionality constant, $A_{\mathrm{NMR}} = 2.2 \times 10^{27}$ m^{-3}/kHz [$v = A_{\mathrm{NMR}} D_{res}/2\pi$]. Based on this independently determined constant, we can estimate the cross-link density v of the composites characterizing the rubber matrix in absolute units [Figure 6E]. We observe that the crosslink density in the polymer phase does not change significantly across morphologies and NP loadings. Furthermore, the crosslink density of the composites are similar to that of the neat polymer with the same level of DCP loading. This proves that all the samples have uniform crosslink density across the polymer phase, irrespective of the NP loading or distance from the NP surface. The lack of a significant amount of constrained immobile chains close to the NP surface as well as distribution tails related to $\frac{1}{M_{graft}}$ suggests that the reinforcement in the sheet like aggregated samples (samples D and E) is likely not due to a fully developed immobilized polymer layer, trapped entanglements or variable crosslink density. These conclusions must be placed in the context of previous studies by Mujtaba *et al*., who found in agreement with simulations that even minute amounts of immobilized material located in the vicinity of particle-particle contacts can account for negative temperature dependent reinforcement by the filler network. In our samples, we observe temperature dependent behavior only in sample D at very high loadings. Thus, for this sample we conclude decisively that the decrease of modulus with temperature (above the glass transition) is caused by energetic effects. However, the source of this enthalpic effect (NP core-core interactions vs. glassy polymer layers) is not conclusively resolved.

4. Discussion

Filler networking, formed by filler-filler and filler-polymer interactions, play a critical role in determining the dynamic properties in filled rubber.[25] NMR suggests that we do not have a fully developed immobilized layer, but the minute quantities of immobile polymer in the vicinity of particle-particle contacts could affect the mechanical reinforcement in some morphologies more strongly than the others. There is no measurable variation in average crosslink density in the polymer phase across the composites. We also observed that reinforcement does not follow the same monotonic trend as S*. Lowering the S* progressively increases van der Waals attractions between the NPs. If S^* (and subsequent strong filler-filler interactions) were the only determinant of reinforcement, then the samples with the lowest S^* would be maximally reinforced. Thus, the question that arises is why (and how) morphologies at intermediate X affect reinforcement

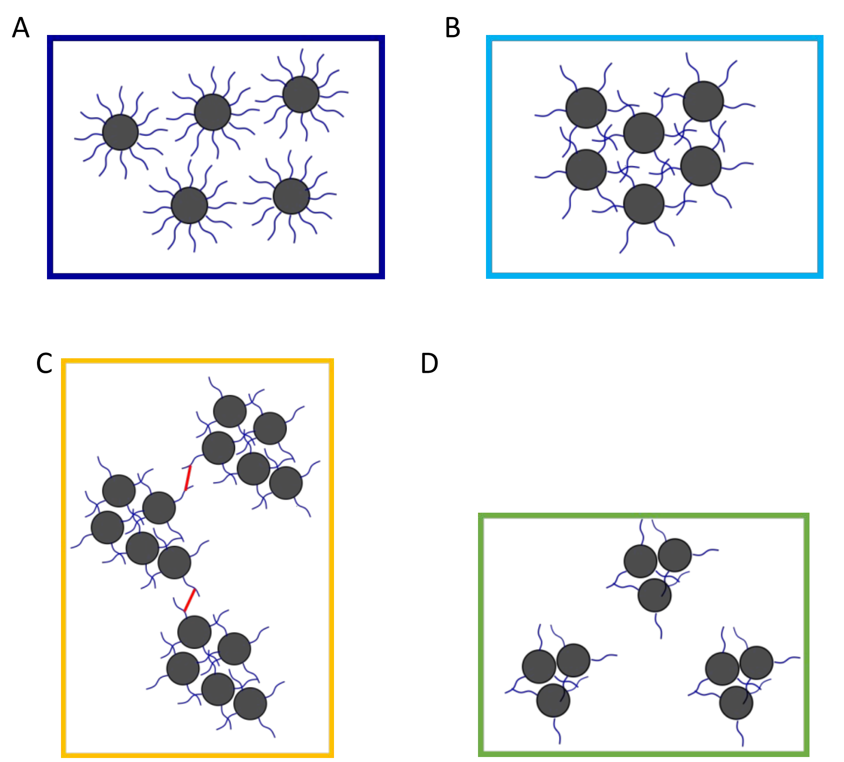

Figure 7: Illustrations of: (A) dense brush screening core-core interactions in sample A, (B) entangled graft chains in sample B, (C) crosslinks (red lines) connecting sheets of NPs, and (D) small clusters dispersed in the system

significantly more than the morphologies at the high and low X limit. Previous work in the melt state has shown that percolation of NPs is important for stress propagation and reinforcement. Below the percolation threshold the individual particles and the isolated aggregates are dispersed in the polymer matrix. All the morphologies at these low NP loadings show similar weak reinforcement. Depending on how stress transfers in the different morphologies, they percolate at different NP loadings.

In the high X limit (sample A), the NPs are well dispersed and completely shielded from each other by the dense brush [Figure 7A]. This random NP dispersion yields the desired percolation effect but only at high NP loadings. As we lower X (samples B and C), the brush is less dense as compared to the well dispersed samples, implying weaker brush-brush repulsion. In all these three cases, the surface is completely covered ($S^*=1$), indicating that filler-filler attractions are screened. In the melt state, we showed that sample B has the highest reinforcement and lowest percolation threshold amongst the morphologies studied.[41, 42] This is because the NPs have higher strength relative to the polymer and hence a percolating NP structure offers the most facile means of stress propagation. The stress transfer between NPs is facilitated by the entanglement of graft chains – thus, for optimal stress transfer we need a percolated NP state but with sufficient S^* to ensure that the chain connectivity can facilitate this process [Figure 7B]. In the crosslinked state, we see that the X value for samples showing the highest reinforcement (samples D and E) are lower than in the melt analog.

At the intermediate X (samples D and E), the particle cores are in contact with one another while having enough graft chains to "entangle" and crosslink. Here we observe that surface is not completely covered by the brush ($S^*<1$), resulting in stronger filler-filler interactions. Thus, attractive forces dominate (either through Van der Waals forces or possible via the small amounts of polymer constraints). In the melt state, samples D and E showed poor reinforcement likely because there were enough graft chains to ensure stress propagation. Once crosslinked, on the other hand, the sheets of aggregates are connected to one another via the crosslinked polymer network to form a continuous network [Figure 7C]. This results in the improved stress transfer in a percolated NP state, and significantly improve reinforcement.[57] The filler network and crosslinked polymer network together carry the load.

The sample lying at the lowest X region contains very few graft chains on the particle surface, yields small NP clusters [Figure 7D]. Here the filler-filler interactions are very strong due to the less surface coverage (S^*=0.69). But the lack of graft chains does not allow optimal stress transfer. Since this morphology is similar to the well dispersed case in that it only percolates at large loadings, it is not surprising that mechanical reinforcement is poor.

4. Conclusion

We have used a combination of different techniques to understand the reinforcement behavior in filled elastomers. The use of grafted particles helps us design systems *a priori* with controlled NP morphologies. We studied the evolution of the morphologies during crosslinking and compared the mechanical properties in the linear and nonlinear regime. In both the high and low X limit, we do not observe a percolation of NPs (till ~20wt% NP loading) that is necessary for reinforcement. We show that, at intermediate X, the formation of sheet like structures connected to each other via a network of crosslinked polymer chains is responsible for the enhanced reinforcement in elastomer composites. In the melt state, the formation of a percolated network with enough entangled grafts (sample B) results in higher reinforcement. This then results in us questioning why sample B is worse than samples D and E in terms of mechanical reinforcement. Here we point to the role of enthalpic interactions which should be larger for samples D/E vs sample B. These results emphasize the important role of the NP surface in determining the moduli of crosslinked elastomers. This last aspect is a unique aspect of crosslinked elastomers, a phenomenon apparently not relevant for the corresponding uncrosslinked melts.

The source of enthalpic interactions can either be through core-core interactions or the creation of adsorbed glassy layers that bridge NPs. While we conclusively cannot decide which of these two energetic mechanisms dictate reinforcement, our results in the nonlinear regime (in the shear and tensile mode) suggest that core-core interactions play a stronger role. The ultimate properties of the crosslinked materials track the melt state reinforcement behavior suggesting that the enthalpic interactions in the crosslinked states do not persist out to larger strains. For sample D, we observe slightly lower toughness as compared to B. If presence of immobilized layers was dictating reinforcement, we would have observed an increase in toughness (especially at the higher loadings). Our work on Payne effect measurements at different temperatures, which will be discussed in a future paper, further suggests that we don't have significant immobile polymer fractions close to the NPs to significantly affect reinforcement. We performed amplitude sweeps at 30^{o}C and 60^{o}C and observed almost identical responses, suggesting a lack of softening of any glassy polymer layer. Hence, we conclude that the percolation and resultant reinforcement is driven by stronger filler-filler interactions where stress is propagated by crosslinked polymer network. In summary, percolation of NPs is critical to reinforcement and the percolation threshold is dictated by the morphology.

Supporting Information. TEM images. Crosslink density calculation

AUTHOR INFORMATION

Authors contribution

The manuscript was written with contributions from all authors. All authors have approved the final version of the manuscript.

Corresponding Authors

* sk2794@columbia.edu

Funding

This work was supported by grant NSF (2124814).

Notes

The authors declare no competing financial interests.

References

(1) Dibbanti, M. K.; Mauri, M.; Mauri, L.; Medaglia, G.; Simonutti, R. Probing small network differences in sulfur-cured rubber compounds by combining nuclear magnetic resonance and swelling methods. *J Appl Polym Sci* **2015**, *132* (43), n/a-n/a. DOI: 10.1002/app.42700.
(2) Mary, C.; Philippon, D.; Lafarge, L.; Laurent, D.; Rondelez, F.; Bair, S.; Vergne, P. New Insight into the Relationship Between Molecular Effects and the Rheological Behavior of Polymer-Thickened Lubricants Under High Pressure. *Tribology Letters* **2013**, *52* (3), 357-369. DOI: 10.1007/s11249-013-0214-y.
(3) Pérez-Aparicio, R.; Vieyres, A.; Albouy, P.-A.; Sanséau, O.; Vanel, L.; Long, D. R.; Sotta, P. Reinforcement in Natural Rubber Elastomer Nanocomposites: Breakdown of Entropic Elasticity. *Macromolecules* **2013**, *46* (22), 8964-8972. DOI: 10.1021/ma401910c.
(4) Mujtaba, A.; Keller, M.; Ilisch, S.; Radusch, H. J.; Thurn-Albrecht, T.; Saalwachter, K.; Beiner, M. Mechanical Properties and Cross-Link Density of Styrene-Butadiene Model Composites Containing Fillers with Bimodal Particle Size Distribution. *Macromolecules* **2012**, *45* (16), 6504-6515. DOI: 10.1021/ma300925p.
(5) Wang, M.-J. Effect of polymer-filler and filler-filler interactions o dynamic properties of filled vulcanizates. *Rubber Chemistry and Technology* **1998**, *71* (3), 520-589.
(6) Vieyres, A.; Pérez-Aparicio, R.; Albouy, P.-A.; Sanseau, O.; Saalwächter, K.; Long, D. R.; Sotta, P. Sulfur-Cured Natural Rubber Elastomer Networks: Correlating Cross-Link Density, Chain Orientation, and Mechanical Response by Combined Techniques. *Macromolecules* **2013**, *46* (3), 889-899. DOI: 10.1021/ma302563z.
(7) Gusev, A. A. Micromechanical Mechanism of Reinforcement and Losses in Filled Rubbers.pdf. *Macromolecules* **2006**, *39* (18), 5960-5962.
(8) Heinrich, G.; Kluppel, M.; Vilgis, T. A. Reinforcement of elastomers. *Current Opinion in Solid State & Materials Science* **2002**, *6* (3), 195-203. DOI: Pii S1359-0286(02)00030-X.

(9) Montes, H.; Lequeux, F.; Berriot, J. Influence of the glass transition temperature gradient on the nonlinear viscoelastic behavior in reinforced elastomers. *Macromolecules* **2003**, *36* (21), 8107-8118. DOI: 10.1021/ma0344590.
(10) Sotta, P.; Albouy, P.-A.; Abou Taha, M.; Long, D. R.; Grau, P.; Fayolle, C.; Papon, A. Nonentropic Reinforcement in Elastomer Nanocomposites. *Macromolecules* **2017**, *50* (16), 6314-6322. DOI: 10.1021/acs.macromol.7b00698.
(11) Heinrich, G. K., M.;. *Recent Advances in the Theory of Filler Networking in Elastomers.pdf*; Springer, 2002.
(12) Meyer, J.; Hentschke, R.; Hager, J.; Hojdis, N. W.; Karimi-Varzaneh, H. A. Molecular Simulation of Viscous Dissipation due to Cyclic Deformation of a Silica-Silica Contact in Filled Rubber. *Macromolecules* **2017**, *50* (17), 6679-6689. DOI: 10.1021/acs.macromol.7b00947.
(13) Salaniwal, S.; Kumar, S. K.; Douglas, J. F. Amorphous solidification in polymer-platelet nanocomposites. *Physical Review Letters* **2002**, *89*, 258301.
(14) Zhu, Z. T., T.; Wang, S.Q.; Meerwall, E.D.; Halasa, A. Investigating Linear and Nonlinear Viscoelastic Behavior Using Model Silica-Particle-Filled Polybutadiene.pdf. *Macromolecules* **2005**, *38*, 8816-8824.
(15) Sternstein, S. S.; Zhu, A. J. Reinforcement mechanism of nanofilled polymer melts as elucidated by nonlinear viscoelastic behavior. *Macromolecules* **2002**, *35* (19), 7262-7273. DOI: 10.1021/ma020482u.
(16) Aguiar da Silva, C.; Nagaraja, S. M.; Weydert, M.; Beiner, M. Diblock-Copolymer-Based Composites for Tire-Tread Applications with Improved Filler Network Topology. *Acs Appl Nano Mater* **2018**, *1* (3), 1003-1008. DOI: 10.1021/acsanm.7b00313.
(17) Merabia, S.; Sotta, P.; Long, D. R. A Microscopic Model for the Reinforcement and the Nonlinear Behavior of Filled Elastomers and Thermoplastic Elastomers (Payne and Mullins Effects). *Macromolecules* **2008**, *41* (21), 8252-8266. DOI: Doi 10.1021/Ma8014728.
(18) Nagaraja, S. M.; Mujtaba, A.; Beiner, M. Quantification of different contributions to dissipation in elastomer nanoparticle composites. *Polymer* **2017**, *111*, 48-52. DOI: 10.1016/j.polymer.2017.01.011.
(19) Mujtaba, A.; Keller, M.; Ilisch, S.; Radusch, H. J.; Beiner, M.; Thurn-Albrecht, T.; Saalwachter, K. Detection of Surface-Immobilized Components and Their Role in Viscoelastic Reinforcement of Rubber-Silica Nanocomposites. *ACS Macro Lett* **2014**, *3* (5), 481-485. DOI: 10.1021/mz500192r.
(20) Botti, A.; Pyckhout-Hintzen, W.; Richter, D.; Urban, V.; Straube, E. A microscopic look at the reinforcement of silica-filled rubbers. *Journal of Chemical Physics* **2006**, *124* (17). DOI: 174908
Artn 174908.
(21) Botti, A.; Pyckhout-Hintzen, W.; Richter, D.; Urban, V.; Straube, E.; Kohlbrecher, J. Silica filled elastomers: polymer chain and filler characterization in the undeformed state by a SANS-SAXS approach. *Polymer* **2003**, *44* (24), 7505-7512.
(22) Krutyeva, M.; Wischnewski, A.; Monkenbusch, M.; Willner, L.; Maiz, J.; Mijangos, C.; Arbe, A.; Colmenero, J.; Radulescu, A.; Holderer, O.; et al. Effect of Nanoconfinement on Polymer Dynamics: Surface Layers and Interphases. *Physical Review Letters* **2013**, *110* (10). DOI: 10.1103/PhysRevLett.110.108303.
(23) Berriot, J.; Montes, H.; Lequeux, F.; Long, D.; Sotta, P. Evidence for the shift of the glass transition near the particles in silica-filled elastomers. *Macromolecules* **2002**, *35* (26), 9756-9762.

(24) Tauban, M.; Delannoy, J.-Y.; Sotta, P.; Long, D. R. Effect of Filler Morphology and Distribution State on the Linear and Nonlinear Mechanical Behavior of Nanofilled Elastomers. *Macromolecules* **2017**, *50* (17), 6369-6384. DOI: 10.1021/acs.macromol.7b00974.
(25) Bokobza, L. The reinforcement of elastomeric networks by fillers. *Macromol Mater Eng* **2004**, *289* (7), 607-621. DOI: 10.1002/mame.200400034.
(26) Montes, H.; Chaussee, T.; Papon, A.; Lequeux, F.; Guy, L. Particles in model filled rubber: Dispersion and mechanical properties. *Eur Phys J E* **2010**, *31* (3), 263-268. DOI: 10.1140/epje/i2010-10570-x.
(27) Cattinari, G.; Steenkeste, K.; Leveque-Fort, S.; Cabriel, C.; Deniset-Besseau, A.; Canette, A.; Oberdisse, J.; Gallopin, M.; Couty, M.; Fontaine-Aupart, M. P. Nanostructural Evolution of Natural Rubber/Silica Nanoparticle Coagulation from Binary Colloidal Suspensions to Composites: Implications for Tire Materials. *Acs Appl Nano Mater* **2021**, *4* (7), 6722-6733. DOI: 10.1021/acsanm.1c00725.
(28) Baeza, G. P.; Genix, A.-C.; Degrandcourt, C.; Petitjean, L.; Gummel, J.; Schweins, R.; Couty, M.; Oberdisse, J. Effect of Grafting on Rheology and Structure of a Simplified Industrial Nanocomposite Silica/SBR. *Macromolecules* **2013**, *46* (16), 6621-6633. DOI: 10.1021/ma401016d.
(29) Baeza, G. P.; Genix, A. C.; Degrandcourt, C.; Petitjean, L.; Gummel, J.; Couty, M.; Oberdisse, J. Multiscale Filler Structure in Simplified Industrial NanocompositeSilica/SBR Systems Studied by SAXS and TEM. *Macromolecules* **2013**, *46* (1), 317-329.
(30) Bouty, A.; Petitjean, L.; Chatard, J.; Matmour, R.; Degrandcourt, C.; Schweins, R.; Meneau, F.; Kwasniewski, P.; Boue, F.; Couty, M.; et al. Interplay between polymer chain conformation and nanoparticle assembly in model industrial silica/rubber nanocomposites. *Faraday Discussions* **2016**, *186*, 325-343. DOI: 10.1039/c5fd00130g.
(31) Bouty, A.; Petitjean, L.; Degrandcourt, C.; Gummel, J.; Kwasniewski, P.; Meneau, F.; Boue, F.; Couty, M.; Jestin, J. Nanofiller Structure and Reinforcement in Model Silica/Rubber Composites: A Quantitative Correlation Driven by Interfacial Agents. *Macromolecules* **2014**, *47* (15), 5365-5378. DOI: 10.1021/ma500582p.
(32) Berriot, J.; Lequeux, F.; Montes, H.; Pernot, H. Reinforcement of model filled elastomers: experimental and theoretical approach of swelling properties. *Polymer* **2002**, *43* (23), 6131-6138. DOI: Pii S0032-3861(02)00553-0
Doi 10.1016/S0032-3861(02)00553-0.
(33) Bonnevide, M.; Jimenez, A. M.; Dhara, D.; Phan, T. N. T.; Malicki, N.; Abbas, Z. M.; Benicewicz, B.; Kumar, S. K.; Couty, M.; Gigmes, D.; et al. Morphologies of Polyisoprene-Grafted Silica Nanoparticles in Model Elastomers. *Macromolecules* **2019**, *52* (20), 7638-7645. DOI: 10.1021/acs.macromol.9b01479.
(34) Akcora, P.; Liu, H.; Kumar, S. K.; Moll, J.; Li, Y.; Benicewicz, B. C.; Schadler, L. S.; Acehan, D.; Panagiotopoulos, A. Z.; Pryamitsyn, V.; et al. Anisotropic self-assembly of spherical polymer-grafted nanoparticles. *Nat Mater* **2009**, *8* (4), 354-U121. DOI: 10.1038/Nmat2404.
(35) Chevigny, C.; Dalmas, F.; Di Cola, E.; Gigmes, D.; Bertin, D.; Boue, F.; Jestin, J. Polymer-Grafted-Nanoparticles Nanocomposites: Dispersion, Grafted Chain Conformation, and Rheological Behavior. *Macromolecules* **2011**, *44* (1), 122-133. DOI: 10.1021/ma101332s.
(36) Srivastava, S.; Agarwal, P.; Archer, L. A. Tethered nanoparticle-polymer composites: phase stability and curvature. *Langmuir* **2012**, *28* (15), 6276-6281. DOI: 10.1021/la2049234.

(37) Moll, J.; Kumar, S. K.; Snijkers, F.; Vlassopoulos, D.; Rungta, A.; Benicewicz, B. C.; Gomez, E.; Ilavsky, J.; Colby, R. H. Dispersing Grafted Nanoparticle Assemblies into Polymer Melts through Flow Fields. *ACS Macro Letters* **2013**, *2* (12), 1051-1055. DOI: 10.1021/mz400447k.
(38) Jouault, N. V. P. D. F. S., S.; Jestin, J.; Boue,F. Well-Dispersed Fractal Aggregates as Filler in Polymer-Silica Nanocomposites: Long-Range Effects in Rheology. *Macromolecules* **2009**, *42*, 2031-2040.
(39) Baeza, G. P.; Genix, A. C.; Degrandcourt, C.; Gummel, J.; Couty, M.; Oberdisse, J. Mechanism of aggregate formation in simplified industrial silica styrene-butadiene nanocomposites: effect of chain mass and grafting on rheology and structure. *Soft Matter* **2014**, *10* (35), 6686-6695. DOI: 10.1039/c4sm01095g.
(40) Akcora, P.; Kumar, S. K.; Moll, J.; Lewis, S.; Schadler, L. S.; Li, Y.; Benicewicz, B. C.; Sandy, A.; Narayanan, S.; Illavsky, J.; et al. "Gel-like" Mechanical Reinforcement in Polymer Nanocomposite Melts. *Macromolecules* **2010**, *43* (2), 1003-1010. DOI: 10.1021/ma902072d.
(41) Dhara, D.; Rahman, M. A.; Abbas, Z.; Ruzicka, E.; Benicewicz, B.; Kumar, S. K. Melt State Reinforcement of Polyisoprene by Silica Nanoparticles Grafted with Polyisoprene. *ACS Macro Lett* **2022**, 1325-1330. DOI: 10.1021/acsmacrolett.2c00507.
(42) Moll, J. F.; Akcora, P.; Rungta, A.; Gong, S. S.; Colby, R. H.; Benicewicz, B. C.; Kumar, S. K. Mechanical Reinforcement in Polymer Melts Filled with Polymer Grafted Nanoparticles. *Macromolecules* **2011**, *44* (18), 7473-7477. DOI: 10.1021/ma201200m.
(43) Abbas, Z. M.; Tawfilas, M.; Khani, M. M.; Golian, K.; Marsh, Z. M.; Jhalaria, M.; Simonutti, R.; Stefik, M.; Kumar, S. K.; Benicewicz, B. C. Reinforcement of polychloroprene by grafted silica nanoparticles. *Polymer* **2019**, *171*, 96-105. DOI: 10.1016/j.polymer.2019.03.031.
(44) Fan, X.; Xu, H.; Wu, C.; Song, Y.; Zheng, Q. Influences of chemical crosslinking, physical associating, and filler filling on nonlinear rheological responses of polyisoprene. *Journal of Rheology* **2020**, *64* (4), 775-784. DOI: 10.1122/1.5124034 (acccessed 9/11/2023).
(45) Khani, M. M.; Abbas, Z. M.; Benicewicz, B. C. Well-Defined Polyisoprene-Grafted Silica Nanoparticles via the RAFT Process. *J Polym Sci Pol Chem* **2017**, *55* (9), 1493-1501. DOI: 10.1002/pola.28514.
(46) Valentín, J. L.; Posadas, P.; Fernández-Torres, A.; Malmierca, M. A.; González, L.; Chassé, W.; Saalwächter, K. Inhomogeneities and Chain Dynamics in Diene Rubbers Vulcanized with Different Cure Systems. *Macromolecules* **2010**, *43* (9), 4210-4222. DOI: 10.1021/ma1003437.
(47) Miyaji, K.; Sugiyama, T.; Ohashi, T.; Saalwächter, K.; Ikeda, Y. Study on Homogeneity in Sulfur Cross-Linked Network Structures of Isoprene Rubber by TD-NMR and AFM – Zinc Stearate System. *Macromolecules* **2020**, *53* (19), 8438-8449. DOI: 10.1021/acs.macromol.0c01266.
(48) Kumar, S. K.; Jouault, N.; Benicewicz, B.; Neely, T. Nanocomposites with Polymer Grafted Nanoparticles. *Macromolecules* **2013**, *46* (9), 3199-3214. DOI: 10.1021/ma4001385.
(49) Alkhodairi, H.; Russell, S. T.; Pribyl, J.; Benicewicz, B. C.; Kumar, S. K. Compatibilizing Immiscible Polymer Blends with Sparsely Grafted Nanoparticles. *Macromolecules* **2020**, *53* (23), 10330-10338. DOI: 10.1021/acs.macromol.0c02108.
(50) Midya, J.; Rubinstein, M.; Kumar, S. K.; Nikoubashman, A. Structure of Polymer-Grafted Nanoparticle Melts. *Acs Nano* **2020**, *14* (11), 15505-15516. DOI: 10.1021/acsnano.0c06134.
(51) Asai, M.; Cacciuto, A.; Kumar, S. K. Quantitative analogy between polymer-grafted nanoparticles and patchy particles. *Soft matter* **2015**, *11* (4), 793-797.

(52) Asai, M.; Zhao, D.; Kumar, S. K. Accurate estimation of the polymer coverage of hairy nanoparticles. *Soft Matter* **2018**, *14* (38), 7906-7915, 10.1039/C8SM01311J. DOI: 10.1039/C8SM01311J.
(53) Payne, A. R. The dynamic properties of carbon black-loaded natural rubber vulcanizates. Part I. *J Appl Polym Sci* **1962**, *6* (19), 57-63. DOI: 10.1002/app.1962.070061906.
(54) Drozdov, A. D.; Dorfmann, A. The stress-strain response and ultimate strength of filled elastomers. *Comp Mater Sci* **2001**, *21* (3), 395-417. DOI: Doi 10.1016/S0927-0256(01)00154-9.
(55) Maillard, D.; Kumar, S. K.; Fragneaud, B.; Kysar, J. W.; Rungta, A.; Benicewicz, B. C.; Deng, H.; Brinson, L. C.; Douglas, J. F. Mechanical Properties of Thin Glassy Polymer Films Filled with Spherical Polymer-Grafted Nanoparticles. *Nano Letters* **2012**, *12* (8), 3909-3914, Article. DOI: 10.1021/nl301792g.
(56) Maillard, D.; Kumar, S. K.; Fragneaud, B.; Kysar, J. W.; Rungta, A.; Benicewicz, B. C.; Deng, H.; Brinson, L. C.; Douglas, J. F. Mechanical properties of thin glassy polymer films filled with spherical polymer-grafted nanoparticles. *Nano Lett* **2012**, *12* (8), 3909-3914. DOI: 10.1021/nl301792g.
(57) Nguyen, H. K.; Nakajima, K. Evidence of the Transition from a Flexible to Rigid Percolating Network in Polymer Nanocomposites. *Macromolecules* **2022**, *55* (7), 2739-2745. DOI: 10.1021/acs.macrmol.2c00208.
(58) Guth, E. THEORY OF FILLER REINFORCEMENT. *Journal of Applied Physics* **1945**, *16* (1), 20-25.
(59) Papon, A.; Montes, H.; Hanafi, M.; Lequeux, F.; Guy, L.; Saalwachter, K. Glass-Transition Temperature Gradient in Nanocomposites: Evidence from Nuclear Magnetic Resonance and Differential Scanning Calorimetry. *Phys Rev Lett* **2012**, *108* (6). DOI: ARTN 065702
10.1103/PhysRevLett.108.065702.
(60) Baeza, G. P.; Genix, A. C.; Degrandcourt, C.; Gummel, J.; Mujtaba, A.; Saalwachter, K.; Thurn-Albrecht, T.; Couty, M.; Oberdisse, J. Studying Twin Samples Provides Evidence for a Unique Structure-Determining Parameter in Simplifed Industrial Nanocomposites. *ACS Macro Lett* **2014**, *3* (5), 448-452. DOI: 10.1021/mz500137e.
(61) Payne, A. R. The dynamic properties of carbon black loaded natural rubber vulcanizates. Part II. *J Appl Polym Sci* **1962**, *6* (21), 368-372. DOI: 10.1002/app.1962.070062115.
(62) Baeza, G. P.; Dessi, C.; Costanzo, S.; Zhao, D.; Gong, S.; Alegria, A.; Colby, R. H.; Rubinstein, M.; Vlassopoulos, D.; Kumar, S. K. Network dynamics in nanofilled polymers. *Nature Communications* **2016**, *7*. DOI: 10.1038/ncomms11368.
(63) Saalwachter, K.; Herrero, B.; Lopez-Manchado, M. A. Chain order and cross-link density of elastomers as investigated by proton multiple-quantum NMR. *Macromolecules* **2005**, *38* (23), 9650-9660. DOI: 10.1021/ma051238g.
(64) Saalwachter, K. Proton multiple-quantum NMR for the study of chain dynamics and structural constraints in polymeric soft materials. *Prog Nucl Mag Res Sp* **2007**, *51* (1), 1-35. DOI: 10.1016/j.pnmrs.2007.01.001.
(65) Jakisch, L.; Garaleh, M.; Schafer, M.; Mordvinkin, A.; Saalwachter, K.; Bohme, F. Synthesis and Structural NMR Characterization of Novel PPG/PCL Conetworks Based upon Heterocomplementary Coupling Reactions. *Macromol Chem Phys* **2018**, *219* (3). DOI: ARTN 1700327
10.1002/macp.201700327.

(66) Karekar, A.; Pommer, R.; Prem, B.; Czibula, C.; Teichert, C.; Trimmel, G.; Saalwachter, K. NMR-Based Cross-Link Densities in EPDM and EPDM/ULDPE Blend Materials and Correlation with Mechanical Properties. *Macromol Mater Eng* **2022**, *307* (7). DOI: ARTN 2100968
10.1002/mame.202100968.
(67) Chasse, W.; Valentin, J. L.; Genesky, G. D.; Cohen, C.; Saalwachter, K. Precise dipolar coupling constant distribution analysis in proton multiple-quantum NMR of elastomers. *J Chem Phys* **2011**, *134* (4). DOI: Artn 044907
10.1063/1.3534856.
(68) Saleesung, T.; Reichert, D.; Saalwachter, K.; Sirisinha, C. Correlation of crosslink densities using solid state NMR and conventional techniques in peroxide-crosslinked EPDM rubber. *Polymer* **2015**, *56*, 309-317. DOI: 10.1016/j.polymer.2014.10.057.
(69) Syed, I. H.; Stratmann, P.; Hempel, G.; Kluppel, M.; Saalwachter, K. Entanglements, Defects, and Inhomogeneities in Nitrile Butadiene Rubbers: Macroscopic versus Microscopic Properties. *Macromolecules* **2016**, *49* (23), 9004-9016. DOI: 10.1021/acs.macromol.6b01802.